World Journal of Advanced Research and Reviews
eISSN: 2581-9615 CODEN (USA): WJARAI
Cross Ref DOI: 10.30574/wjarr
Journal homepage: https://wjarr.com/

(RESEARCH ARTICLE)

Check for updates

Study of the structural, electronic, optical, and elastic properties of $NaSrX_3$ (X = Br and I) perovskites using Density Functional Theory (DFT) with GGA formalism

Mona Hermann Charly YAPI [1, 2, *], Guy Müller Banquet OKRA [1, 2], Mélèdje C. Désiré [2, 3], Niaré Adama [2] and Kré N. Raymond [2]

[1] *Laboratory of Environmental Sciences and Technologies (LSTE), University JEAN LOROUGNON GUÉDÉ (UJLoG), Daloa, BP 150 Daloa, Côte d'Ivoire.*
[2] *Laboratory of Fundamental and Applied Physics (LPFA), University NANGUI ABROGOUA (UNA), Abidjan, BP 801 Abidjan 02, Côte d'Ivoire.*
[3] *Institute for Research on New Energies (IREN), University NANGUI ABROGOUA (UNA), Abidjan, BP 801 Abidjan 02, Côte d'Ivoire.*

World Journal of Advanced Research and Reviews, 2025, 28(01), 160-174

Publication history: Received on 27 August 2025; revised on 01 October 2025; accepted on 04 October 2025

Article DOI: https://doi.org/10.30574/wjarr.2025.28.1.3432

Abstract

The electronic and optical properties of $NaSrX_3$ (X = Br, I) perovskites using density functional theory (DFT) with GGA (Generalized Gradient Approximation) formalism. The lattice parameters obtained are 5.22 Å and 5.74 Å for $NaSrBr_3$ and $NaSrI_3$, respectively. $NaSrBr_3$ and $NaSrI_3$ have direct gaps of 2.51 eV and 1.49 eV, respectively. They all have a conduction band dominated by 3d statesof Sr, weakly mixed with 3s states of Na and 4s states of Sr. The valence band is dominated by the 2p states of the alkali metal and the 3d states of Sr. These perovskites also have very good optical properties: low reflectivity and high absorption in the ultraviolet. Observation of the different optical functions shows that the materials can slow down and deflect light in both the visible and ultraviolet ranges. Light can also be absorbed in energy ranges corresponding to the visible and UV spectrums. They are also transparent between 10 eV and 20 eV. These materials are suitable for various applications in both the visible and UV spectrums. The elastic properties of $NaSrBr_3$ and $NaSrI_3$ are also very interesting. The elastic constants found verify the criteria for mechanical stability. $NaSrBr_3$ and $NaSrI_3$ are ductile and likely to be ionic. They are anisotropic and stable materials. $NaSrBr_3$ has a higher melting point than $NaSrI_3$. This work confirms that $NaSrBr_3$ and $NaSrI_3$ have very good electronic, optoelectronic, elastic, and optical properties. Their use in a photovoltaic cell could increase its conversion efficiency.

Keywords: DFT; Perovskites; Nasrx3; Electronic; Optical; Elastic

1. Introduction

The world today faces serious energy challenges. Conventional energy sources are being depleted day by day. Added to this is the fact that the very exploitation of these energies poses a real environmental problem. It exacerbates global warming and causes considerable damage to the environment. Other energy sources are therefore needed. The only alternative is to turn to renewable energy sources. Renewable energy offers considerable advantages. The first advantage is that renewable energies have no harmful effects on the environment. Secondly, they are not difficult to exploit. And finally, these sources are inexhaustible. To ensure energy self-sufficiency for humanity, appropriate research in this field should be undertaken immediately. The most promising renewable energy source is photovoltaic energy based on solar cells. Most solar cells are made from silicon. This also has disadvantages: high production costs and the exploitation of silicon, which damages the environment. Other materials are also used. One example is multi-junction solar cells consisting of several thin layers deposited by metal organic vapor phase epitaxy (MOVPE) or

* Corresponding author: Mona Hermann Charly YAPI

molecular beam epitaxy. This type of solar cell achieves a record photo conversion efficiency. We can also mention tandem cells and CIGS cells. However, most of these solar cells have the same disadvantages as silicon cells. If we want to make photovoltaics the ideal candidate for alternative energy, we need to focus our research on other materials. This is why some researchers have turned their attention to perovskite materials. Perovskite cells have seen their efficiency increase to between 18% and 20% in 2015, which is close to that of silicon-based cells (25%) [1,2,3]. Most of these cells are made with organic perovskites. Perovskite solar cells have the advantage of good absorption of the solar spectrum, good flexibility and lightness, and low-temperature manufacturing, which can result in lower production costs. In addition, these materials are very abundant on earth. However, they pose stability problems. Research on these materials must therefore continue, not only to increase the efficiency of these cells, but also to resolve their instability issues. Inorganic perovskites, although they have low conversion efficiency, are nevertheless more stable than organic perovskites. Our work consisted of studying the structural, electronic, optical, and elastic properties of $NaSrX_3$-type perovskites (X = Br and I) using density functional theory (DFT) with GGA formalism.

2. Materials and Methods

2.1. Materials

This work was carried out using Quantum Expresso (qe-7.0) software [4,5,6] running on Ubuntu 25.04 Linux. Quantum-espresso is a software suite consisting of several subprograms that perform specific tasks. We used a Core i7 computer (Lenovo series) with a frequency of 2.90 GHz. We also used other programs to process the data generated by Quantum-espresso. These include Vesta, Gnuplot, and Xmgrace. Quantum Espresso itself contains several subprograms specific to very precise tasks. For this work, we used $NaSrBr_3$ and $NaSrI_3$ perovskites as materials. These materials are supposed to crystallize in a cubic crystal structure (Pm3m). Figure 1 shows a typical representation of the crystal structure of each material. We used five atoms per lattice.

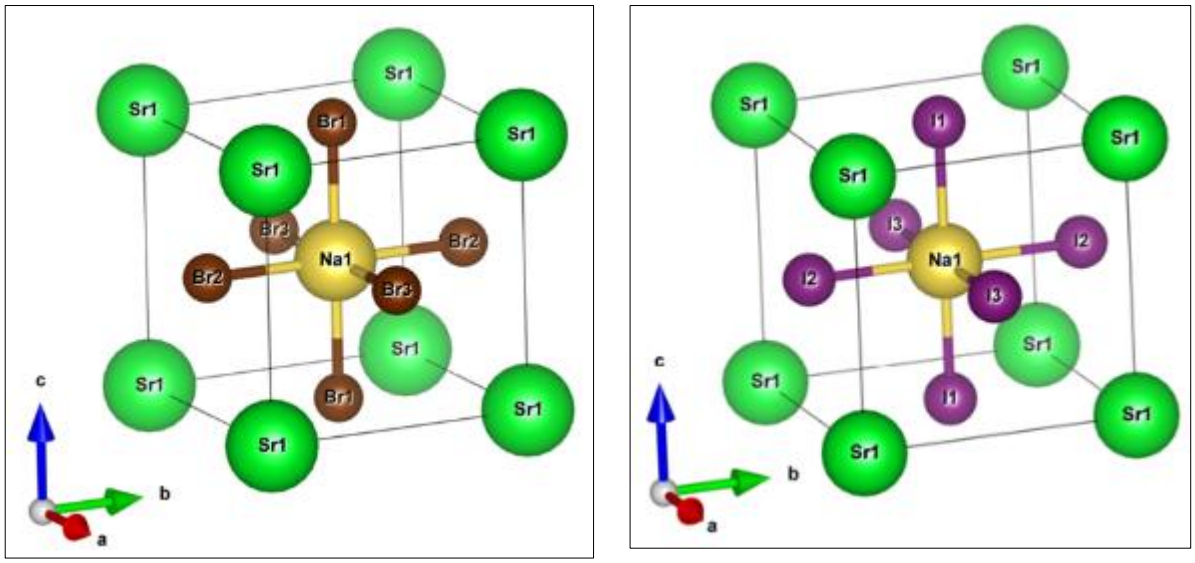

Figure 1 Cubic crystal structure of $NaSrBr_3$ (left) and $NaSrI_3$ (right)

2.2. Méthodes

This work was carried out using density functional theory (DFT), a quantum calculation method. DFT is implemented by the Quantum Espresso code [4,5]. In this study, the DFT formalism used is the generalized gradient approximation (GGA) of Perdew, Burke, and Ernzerhof (PBE + GGA) [7,8,9]. We set the convergence level at 10-9 (1.0d-9 eV). The k points in the Brillouin zone were divided into 12×12×12. The kinetic cutoff energy was set at 80.0 Ry. However, it is important to note that the lattice parameter, kinetic cutoff energy, Monkhorst-Pack k-point sampling in the Brillouin zone, and other parameters of the perovskite material structures were obtained by relaxation.

3. Results and discussion

3.1. Convergence test

We performed convergence tests to determine the optimal equilibrium values for the $NaSrBr_3$ and $NaSrI_3$ perovskite structures under study. These optimized parameters are: lattice parameter, kinetic cutoff energy, and Monkhorst-Pack k-points in the Brillouin zone. The convergence level is 10^{-9} (1.0d-9 eV). This convergence test is performed using the vc_relax calculation. It consists of several iterations of the parameter values considered in order to obtain the most stable system. The most stable system is the one that corresponds to the parameter value that assigns the lowest energy to the material.

3.1.1. Lattice parameter

Figure 2 shows the evolution of the total energy of the system as a function of the evolution of the lattice parameter of $NaSrBr_3$ and $NaSrI_3$.

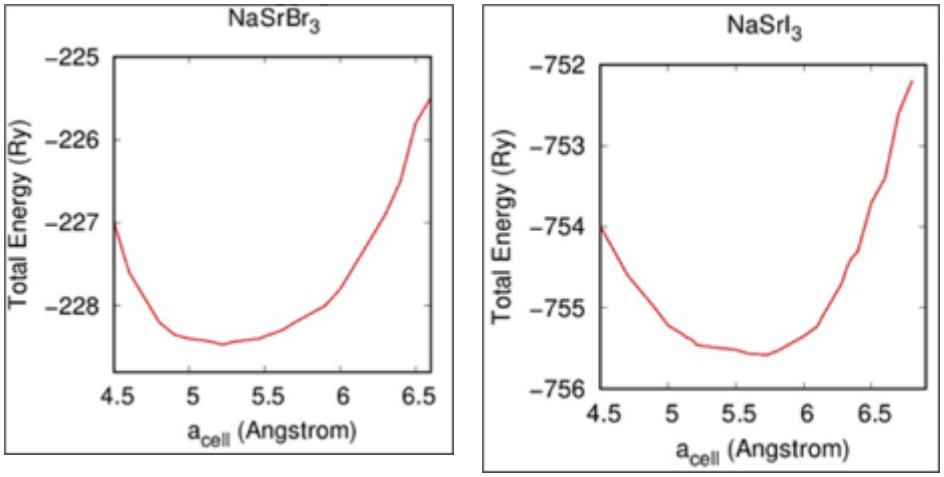

Figure 2 Convergence of Lattice Parameter a_{cell}.

Table 1 shows the different lattice parameter values obtained for $NaSrBr_3$ and $NaSrI_3$. $NaSrBr_3$ has a lattice parameter of 5.22 Å and $NaSrI_3$ has a lattice parameter of 5.74 Å. Compared to other authors such as M T Hossain et al [10,11], our lattice parameters are lower.

Table 1 Calculated mesh parameters

Latice parameter a_{cell} in Å		
Materials	**Our results**	**Literature results**
$NaSrBr_3$	5.22	5.86 [10]
$NaSrI_3$	5.74	6.47 [11]

3.2. Convergence of Kinetic energy cut-off

The cutoff kinetic energy (ecut) represents the kinetic energy of the electron wave function in the crystal that the latter cannot reach [4,5,12]. It is a limit that is set for each iteration. The relaxation of this quantity gave us 70 Ry, but for greater precision we chose a value above 70 Ry, i.e., 80 Ry. In fact, the higher this quantity, the more accurate the calculations will be. But in this case, the computing resources required will be enormous, as will the calculation time. In their work, M T Hossain et al used 67 Ry for $NaSrBr_3$ [10] and 90 Ry for $NaSrI_3$ [11].

3.3. Convergence of k-point

The k points of the Brillouin zone of the perovskites NaSrBr3 and $NaSrI_3$ were sampled using the Monkhorst-Pack method [13]. The relaxation of the k points shows a convergence of 6×6×6. However, we chose to set our Monkhorst-

Pack grid to 12×12×12. We consider this sampling to be very relevant for these calculations. However, given that it is high, the computing resources and calculation time required will be enormous. It is well known in the literature that the k-point grid is very relevant from 8×8×8 onwards.

3.4. Electronic properties

3.4.1. Bands structure

The electronic properties of the perovskite materials $NaSrBr_3$ and $NaSrI_3$ obtained are presented and discussed in this section. These electronic properties concern: the electronic band structure, the total density of states (TDOS) and partial densities of states (PDOS), and the charge density of the cubic perovskites $NaSrBr_3$ and $NaSrI_3$. The band structure is calculated according to the high symmetry direction of the first Brillouin zone on the path M-Γ-M-R-X-R-M. The band structure is crucial for describing the magnetic, electronic, optical, and thermal properties of a material [14]. Figure 3 shows the electronic band structure of $NaSrBr_3$ and $NaSrI_3$.

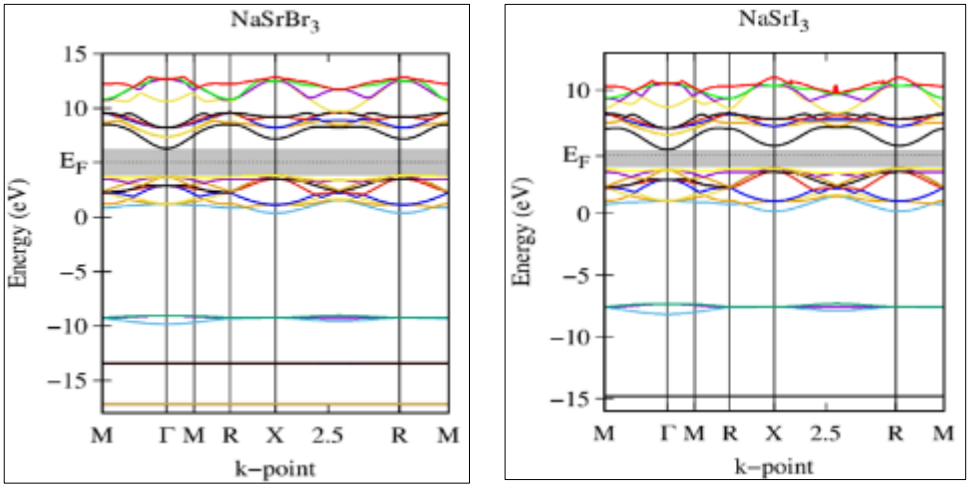

Figure 3 Electronic band structure of $NaSrBr_3$ and $NaSrI_3$

The electronic band structure provides information on the nature of the material: whether it is a conductor, semiconductor, or insulator. It evaluates the energies at which electrons are present in the different energy bands. It also indicates the different regions where electrons are available. The band structure has two very important bands. The valence band (VB) and the conduction band (CB) are two neighboring bands but with different energy bands arranged one above the other. The conduction band is above and the valence band is below. Between these two is the Fermi energy level (EF). The gap is the distance between the minimum of the conduction band and the maximum of the valence band. It is this distance between the conduction band and the valence band, or gap, that determines whether a material is a conductor, semiconductor, or insulator. The wider the gap, the more insulating the material is. The material is conductive if the gap is zero. Sometimes the gap is very small, i.e., less than 5 eV, in which case the material is a semiconductor [14,15]. Table 2 shows the gap obtained for cubic $NaSrX_3$ (X= Br and I) perovskite materials.

Table 2 Gap values obtenir for pérovskites $NaSrX_3$ (X= Br and I)

Gap values in eV		
Materials	**Our results**	**Literature results**
$NaSrBr_3$	2.51	2.95 [10]
$NaSrI_3$	1.49	2.41 [11]

$NaSrBr_3$ and $NaSrI_3$ have band gaps of 2.51 eV and 1.49 eV, respectively, which are less than 5 eV. $NaSrBr_3$ and $NaSrI_3$ are therefore semiconductors. M T Hossain et al [10] obtained a band gap of 2.95 eV for $NaSrBr_3$, compared to 2.51 eV for us, and 2.41 eV for $NaSrI_3$ [11], compared to 1.49 eV for us. The band gap values obtained for $NaSrBr_3$ and $NaSrI_3$ in our work are much lower than those obtained by M T Hossain et al [10, 11] in their work. The band gaps obtained in our work are all direct on the Γ-Γ path. These materials can therefore be used in electronic and optoelectronic applications.

3.5. Partial and total densities of state

The density of states (DOS) and total and partial densities of states (PDOS) provide insight into the contribution of different atomic orbitals to the density of states (DOS) and the nature of bonds in materials. Figure 4 shows the partial densities of states for $NaSrX_3$-type perovskite materials (X = Br and I). In the $NaSrBr_3$ material, the valence band is characterized by the 2p state of Br weakly mixed with the 5p states of Sr and 3d states of Sr. The conduction band is characterized by the 3d state of Sr, 4s of Sr, and 5p of Sr. In the $NaSiI_3$ material, the valence band is characterized by the 2p state of I weakly mixed with the 3d state of Sr and 5p of Sr. The conduction band is characterized by the 3d state of Sr, 4s of Sr, and 4s of Sr. In this conduction band, the contribution of the 3d state of Sr is very strong. Based on the above, the valence band of $NaSrX_3$-type perovskite materials (X = Br and I) is characterized by the 2p state of the halogen present weakly mixed with other states.

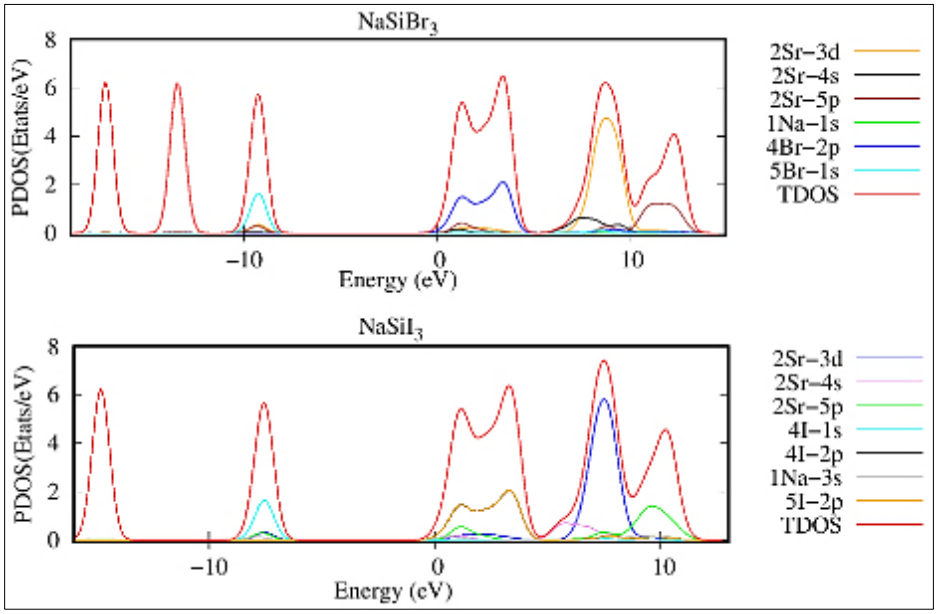

Figure 4 Calculated total and partial densities of states for $NaSrX_3$ (X = Br and I)

The bottom of the conduction bands is dominated by the 3d states of Sr. Observing the boundaries of the valence band and conduction band of the materials studied, band overflows appear. These observations are presented in Figure 5. The graphs in figure 5 show the maximum valence band energy (E_V), the minimum conduction band energy (E_C), and the Fermi level (E_F). The Fermi level E_F of $NaSrBr_3$ is located almost halfway between the conduction band and the valence band. In $NaSrI_3$, the Fermi level E_F is closer to the conduction band. Each graph shows band overlap in the band gap. These band overlaps are likely to reduce the gap in the event of doping. In $NaSrBr_3$, it is the 2p of Br and the 4s of Sr that spill over into the band gap. In $NaSrI_3$, the spillover is due to the 2p state of I. In the latter case, the 2p state completely crosses the band gap. $NaSrI_3$ is therefore almost a conductor.

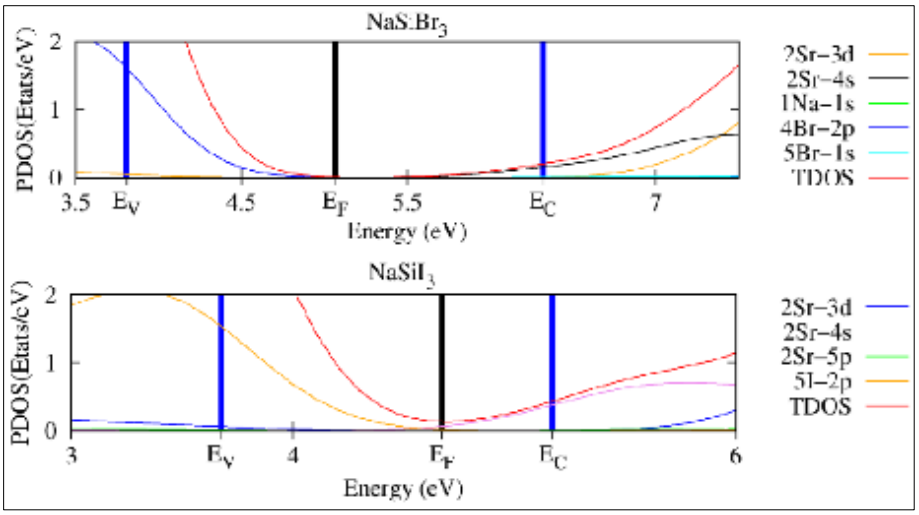

Figure 5 The edges of bands of calculated state densities for $NaSrBr_3$ ande $NaSrI_3$

In order to better understand the nature of the bond between the different atoms contained in a material, its charge density must be observed. Figures 6 and 7 show the charge densities of $NaSrBr_3$ and $NaSrI_3$ in the crystallographic directions (110) and (100), respectively.

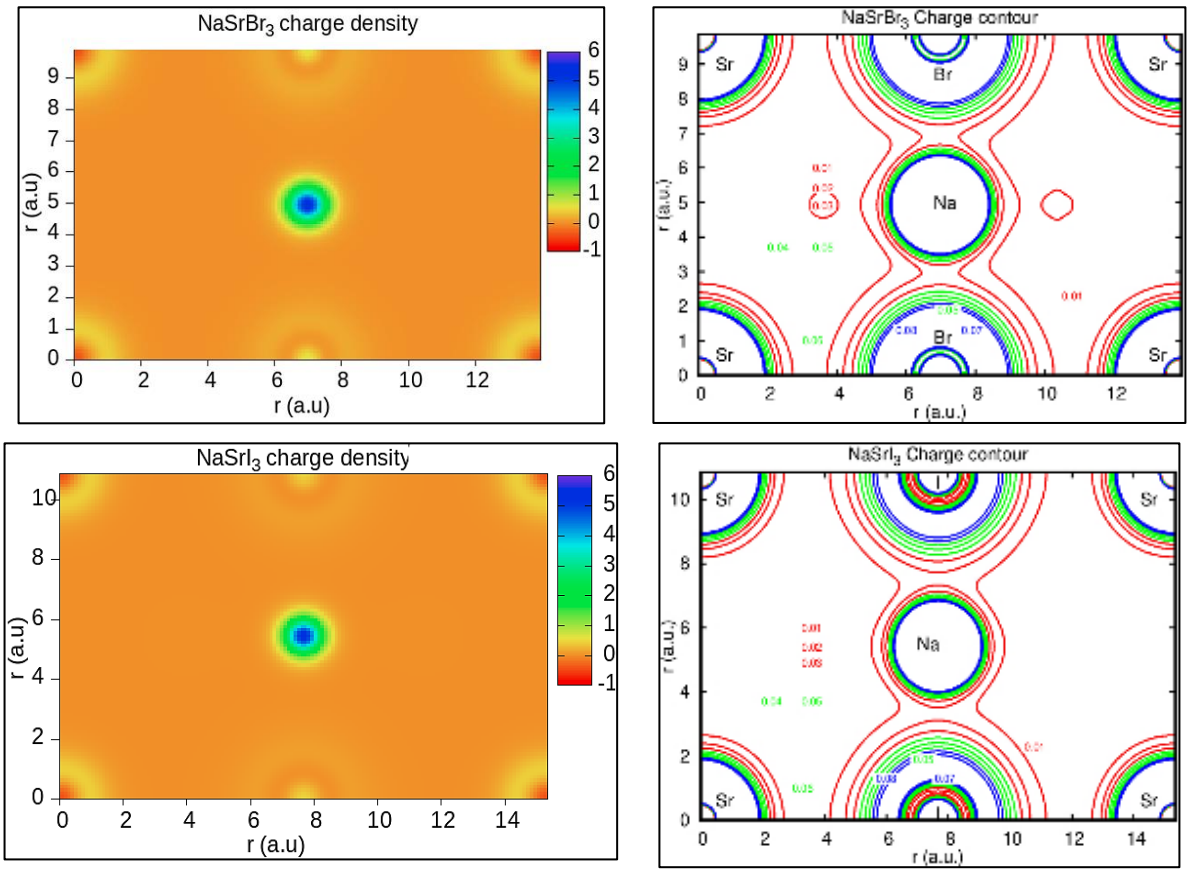

Figure 6 Charge denssity of $NaSrBr_3$ and $NaSrI_3$ in crystallographic plane (110)

The bonding behavior and charge distribution between atoms can be understood using the valence electron charge density derived from convergent wave functions. By observing the map of the variation in the electron charge density of a compound, information can be obtained about the type of bond between the constituents [16]. These charge density graphs show that the density is very high around the halogen atoms, i.e., Br and I. This is undoubtedly due to their high electronegativity compared to the other atoms present in these perovskites.

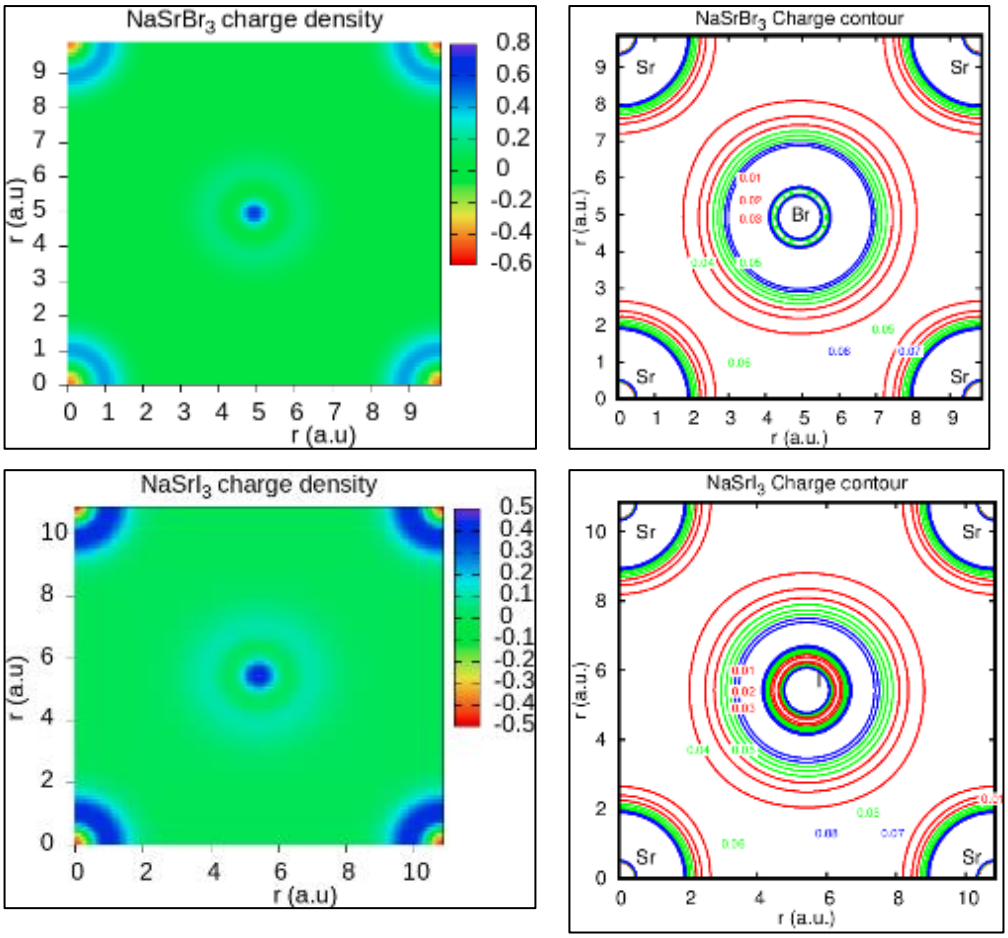

Figure 7 Charge denssity of $NaSrBr_3$ and $NaSrI_3$ in crystallographic plane (100)

The charge distribution is identical in each perovskite material. This charge distribution, as observed on each map, suggests a rather ionic or metallic bond between the Na atom and the alkali metals Br and I. In the (110) crystallographic plane, the distinctive charge distribution suggests a probable hybridization between Na and Br in $NaSrBr_3$ and a hybridization between Na and I in $NaSrI_3$. This therefore indicates a probable covalent Na-Br bond in $NaSrBr_3$ and a probable covalent Na-I bond in $NaSrI_3$. There is therefore a transfer of charges between Na and the alkali corresponding to these perovskites. However, according to the crystallographic plane (100), there will be no covalent bond between Sr and the corresponding alkali of the perovskite in question.

3.6. Optical properties

3.6.1. Real part and imaginary part of the complex dielectric function

Optical properties provide insight into how the material reacts to light. These sought-after optical properties can be deduced from the complex dielectric function $\tilde{\varepsilon}$. It represents the response of the material's electrons when it interacts with light and is written as : $\tilde{\varepsilon}(\omega) = \varepsilon_r(\omega) + i\varepsilon_i(\omega)$. ε_r is real part and ε_i, the imaginary. The imaginary part ε_i is responsible for the absorption of the material, and the real part ε_r is responsible for the polarization of the medium. In this work, the real and imaginary parts of the complex dielectric function of $NaSrBr_3$ and $NaSrI_3$ perovskites are shown in Figure 6. These curves have two parts : from 0 eV to 13 eV and then from 13 eV to 30 eV. Each part is characterized by different fluctuations. The maximum peak of the real part of the dielectric function of the $NaSrBr_3$ and $NaSrI_3$ compounds are positioned at energies of 4.32 eV and 3.28 eV, respectively. As for the imaginary part of the dielectric function of the $NaSrBr_3$ and $NaSrI_3$ compounds, they are positioned at energies of 4.44 eV and 3.64 eV, respectively. For each perovskite compound, the main imaginary peak and the main real peak almost coincide. These different peaks appear to converge at 3.0 eV when moving from the perovskite with the lightest halogen to that with the heaviest halogen.

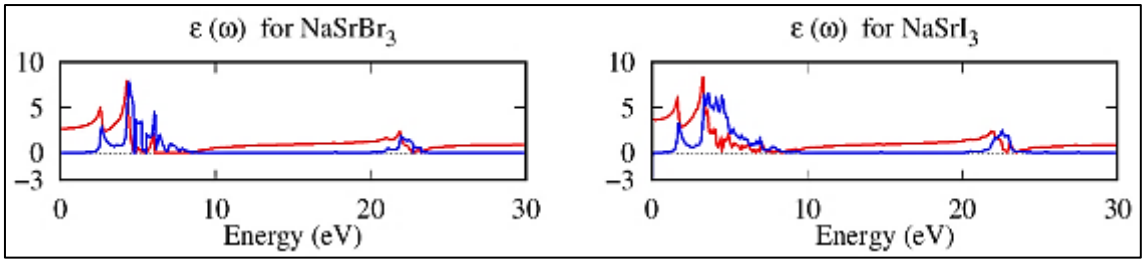

Figure 8 Real part (in red) and imaginary part (in blue) of the dielectric function calculated

3.6.2. Optical functions

Other optical functions can be deduced from the dielectric function. These are: refractive index n(ω), extinction coefficient k(ω), reflection coefficient or reflectivity R(ω), absorption coefficient α(ω), and optical conductivity σ(ω). These optical functions are represented respectively by Figures 7, 8, 9, 10, and 11.

3.7. Refractive index

The complex refractive index is very important for understanding how photons affect the medium during propagation [15, 17]. The real part represents the real refractive index n(ω) in front of the phase velocity of the incident wave. The imaginary part is the extinction coefficient k(ω). The latter represents the reduction in incident light. A large real refractive index indicates slow light propagation and therefore greater deviation. A non-zero imaginary part of the complex refractive index means that light is absorbed by the medium. The wave will then weaken more and more as it propagates. A transparent material has a zero imaginary part and a zero and positive real part. Figure 7 shows the calculated real refractive index n(ω) of the perovskites $NaSrBr_3$ and $NaSrI_3$. Both compounds have positive refractive indices. Two parts can be distinguished: from 0 eV to 8 eV and from 8 eV to 30 eV.

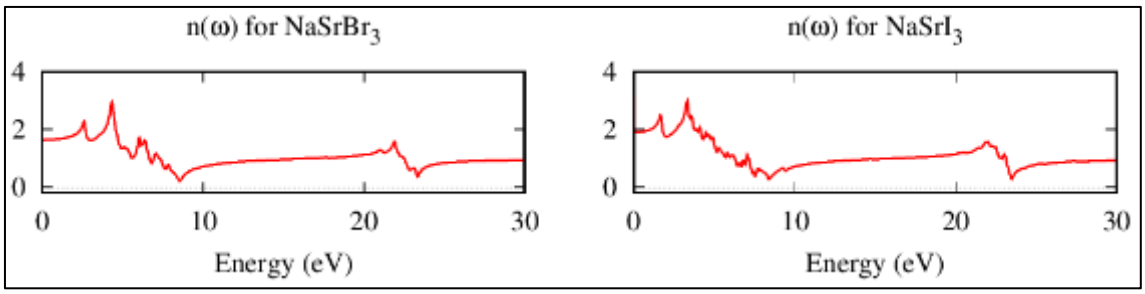

Figure 9 Refractive index for $NaSrBr_3$ and $NaSrI_3$

The refractive indices in these two materials are almost identical from 8 eV to 30 eV. In both materials, since the refractive index is non-zero, light passing through these materials is likely to propagate more slowly and will be more deflected in both the visible and UV ranges. The main peaks are 2.95 to 4.32 eV and 2.98 to 3.33 eV for $NaSrBr_3$ and $NaSrI_3$, respectively. These peaks are therefore almost identical. The static refractive index obtained for each is 1.63 and 3.16 for $NaSrBr_3$ and $NaSrI_3$, respectively. M T Hossain et al obtained 2.2 for $NaSrBr_3$ and 1.57 for $NaSrI_3$. This shows a very significant difference between our two studies.

3.8. Extinction coefficient K(ω)

The extinction coefficient K(ω) is the imaginary part of the complex refractive index. Figure 8 shows the calculated extinction coefficient for the perovskites $NaSrBr_3$ and $NaSrI_3$. The extinction coefficient K(ω) characterizes the attenuation of electromagnetic radiation energy as it passes through the medium. The higher the value of K(ω), the stronger the interaction between the radiation and the material, resulting in greater attenuation of the beam intensity. A non-zero value of K(ω) means that light is absorbed by the medium. The wave will then weaken more and more as it propagates. A transparent material has a zero value of K(ω) and a positive real value of n(ω).

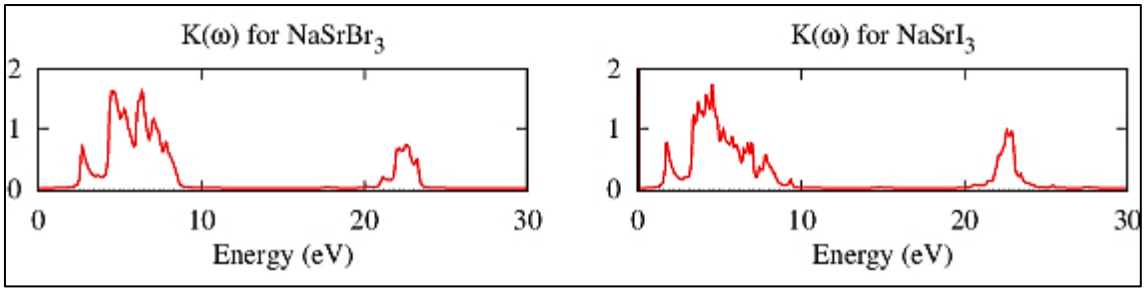

Figure 10 Extinction coefficient for $NaSrX_3$ halide perovskites (X = F, Cl, Br and I)

Looking at these graphs, two parts stand out, which are almost identical in both materials. These are: from 0 eV to 10 eV and from 20 eV to 25 eV. The main peak for $NaSrBr_3$ and $NaSrI_3$ is 4.52 eV. As the value of K(ω) is high between 2 eV and 8 eV, we can conclude that the interaction between radiation and matter is stronger. There is therefore greater attenuation of the light beam intensity. The same observation applies to both materials between 21 eV and 24 eV. Thus, in these two ranges, i.e., from 0 eV to 10 eV and from 20 eV to 25 eV, the value of K(ω) is not zero, meaning that light is absorbed by the material. The light will gradually weaken as it propagates through these materials. Between 10 eV and 20 eV, K(ω) is zero while n(ω) is non-zero. These two materials are therefore transparent between 10 eV and 20 eV. We note that no discussion has been made in the literature on this subject.

3.9. Reflectivity R(ω)

Optical reflectivity characterizes the ability of a surface to reflect the light it receives. It is the ratio of the reflected intensity to that of the incident wave. Figure 9 shows the calculated optical reflectivity R(ω) of the perovskites $NaSrBr_3$ and $NaSrI_3$.

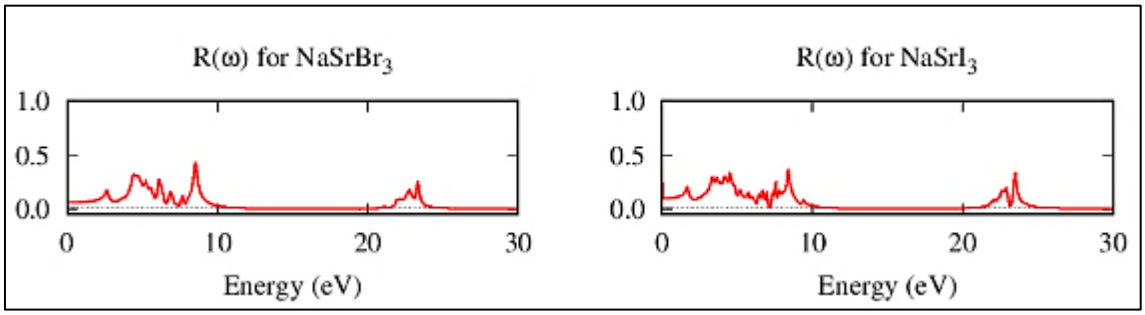

Figure 11 Reflexivity for $NaSrBr_3$ et $NaSrI_3$

The same observation as before can be made. Two parts stand out in these two compounds. These two parts are almost identical in both compounds: from 0 eV to 10 eV and from 20 eV to 24 eV. The main peaks are 0.43 to 8.52 eV and 0.35 to 8.40 eV for $NaSrBr_3$ and $NaSrI_3$, respectively. The static reflectivity values (at 0 eV) are 0.058 and 0.462 for $NaSrBr_3$ and NaSrI3, respectively. M T Hossain et al obtained main peaks at 8.2 eV for $NaSrBr_3$ [10] and at 7.2 eV for $NaSrI_3$ [11] and static reflectivity values at 0 eV of 0.07 for $NaSrBr_3$ [10] and 0.05 for $NaSrI_3$ [11].

3.10. Absorption coefficient α(ω)

The absorption coefficient α(ω) characterizes the decrease in intensity of an incident wave passing through a material. A high absorption coefficient indicates that the material strongly absorbs light, converting it into thermal energy. Such absorption results in low transmission or reflection. A low absorption coefficient indicates that the material is highly transparent. The absorption coefficient also characterizes whether the material is metallic, semiconducting, or insulating. Figure 10 shows the absorption coefficient α(ω) obtained for $NaSrBr_3$ and $NaSrI_3$. Absorption of the two materials begins at 1.50 eV and 1.0 eV for $NaSrBr_3$ and $NaSrI_3$, respectively. Absorption in these two compounds also has two parts: from 1 eV to 10 eV and from 20 eV to 25 eV. The two curves have the same shape and show the same similarity. The main peaks are located exactly at the same energy value, i.e., 4.52 eV for $NaSrBr_3$ and $NaSrI_3$. For these materials, there is absorption in both the visible and ultraviolet ranges.

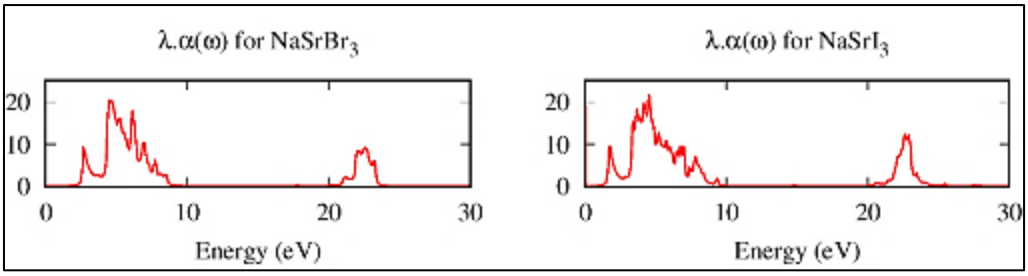

Figure 12 Absorption coefficient for $NaSrBr_3$ et $NaSrI_3$

3.11. Optical conductivity σ(ω)

Optical conductivity σ(ω) explains the transport of electrons when light interacts with matter [18]. Optical conductivity σ(ω) also explains the absorption and polarization of the material at given optical frequencies. Figure 11 shows the optical conductivity σ(ω) calculated for $NaSrBr_3$ and $NaSrI_3$. We can see that at 0 eV, the optical conductivity σ(ω) in both materials is zero. The optical conductivity of each is non-zero from 0.6 eV to 9 eV and from 20 eV to 24 eV. This shows that during light-matter interaction with these materials, electron transport occurs within these energy ranges. The main peaks for each are located at 4.51 eV and 3.74 eV for $NaSrBr_3$ and $NaSrI_3$, respectively.

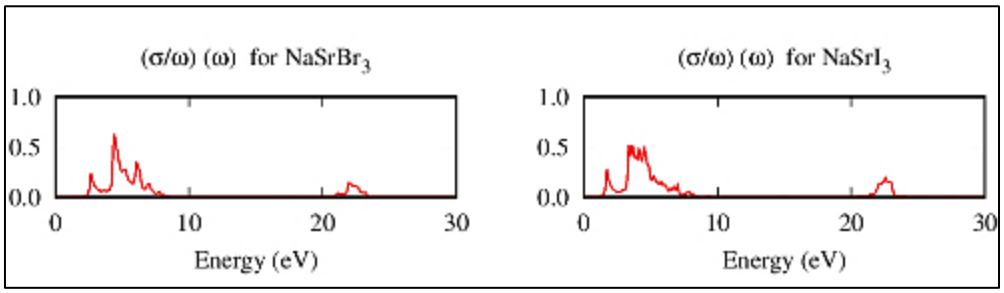

Figure 13 Optical conductivity for $NaSrBr_3$ and $NaSrI_3$

3.12. Energy loss function L(ω)

The energy loss spectrum L(ω) depends on the dielectric function $\tilde{\varepsilon}(\omega)$ and the frequency ω of the incident wave [17]. L(ω) shows the collective excitation spectrum produced by an electron as it passes through the material. The peak of the energy loss spectrum L(ω) appears at a specific frequency (or energy) of the incident light. This frequency is the plasma frequency. It is estimated from the energy loss spectrum. Figure 12 shows the energy loss spectrum of the compounds $NaSrBr_3$ and $NaSrI_3$. The energy region observed is less than 50 eV, so L(ω) corresponds to the valence loss spectrum. In this region, valence electrons cause resonant oscillations. A sharp peak forms when the value of $\varepsilon_i(\omega)$ is very low and $\varepsilon_r(\omega)$ is zero or close to zero [17]. The corresponding frequency is the plasma frequency ε_P. We make the same observation as for the previous optical functions, with the presence of two distinct zones: from 0 eV to 10 eV and from 20 eV to 25 eV. Each zone has a main peak. In the first zone, we have a main peak from 12.09 to 8.56 eV for $NaSrBr_3$ and from 7.95 to 8.40 eV for NaSrI3. In the second zone, there is also a main peak from 4.44 to 23.32 eV for $NaSrBr_3$ and from 7.28 to 23.46 eV for NaSrI3. The largest peaks correspond to the plasma frequency of the material.

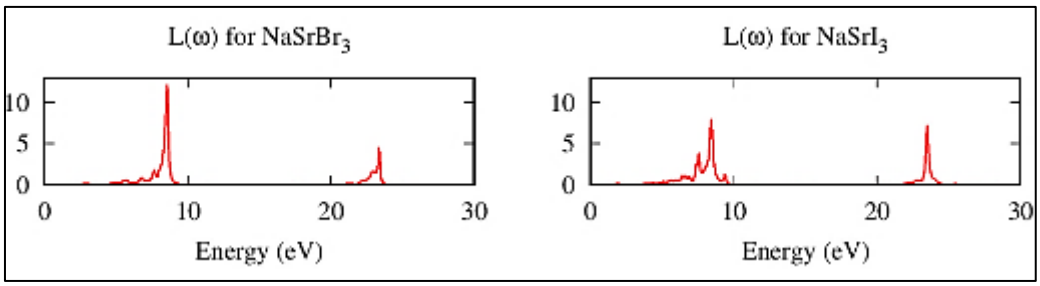

Figure 14 Energy loss function spectrum for $NaSrBr_3$ and $NaSrI_3$

3.13. Elastic properties

Elastic properties describe the mechanical and dynamic behavior of the material. These elastic properties are determined using independent elastic constants. To characterize the elasticity of a cubic symmetry, only three elastic constants are required: C_{11}, C_{12}, and C_{44}. These correspond to the directional mechanical responses of the crystal according to the directions of forces or stresses applied to these materials [19].

3.13.1. Elastic constants

The parameters C_{11}, C_{12}, and C_{44} obtained for the perovskite materials $NaSrBr_3$ and $NaSrI_3$ are shown in Table 3.

Table 1 Elastic constants cubic crystals $NaSrBr_3$ and $NaSrI_3$

	C_{11} (GPa)	C_{12} (GPa)	C_{44} (GPa)	$C_{11}+2C_{12}$ (GPa)	$C_{11}-C_{12}$ (GPa)	$\frac{C_{11}}{C_{12}}$	$\frac{C_{11}}{C_{44}}$
$NaSrBr_3$	104.60	103.32	15.01	311.25	1.28	1.01	6.96
$NaSrI_3$	52.14	51.45	63.84	155.04	0.69	1.01	0.81

The values obtained for C_{11}, C_{12}, and C_{44} are 104.60 GPa, 103.32 GPa, and 15.01 GPa for $NaSrBr_3$, and 52.14 GPa, 51.45 GPa, and 63.84 GPa for $NaSrI_3$. M T Hossain et al obtained values of 38.45 GPa, 3.50 GPa, and 2.65 GPa for C_{11}, C_{12}, and C_{44}, respectively, for NaSrBr3 [10], and values of 30.91 GPa, 4.10 GPa, and 2.04 GPa for C_{11}, C_{12}, and C_{44}, respectively [11]. C_{11} reflects unidirectional compression along the crystallographic directions [20,21,22]. C_{11} is higher than C_{12} and C_{44} in $NaSrBr_3$. This therefore reflects a lower resistance to pure shear deformation compared to unidirectional compression resistance. In $NaSrI_3$, C_{11} is lower than C_{44}. We are therefore not dealing with a lower resistance to pure shear deformation. The elastic constants satisfy the mechanical stability criteria for cubic crystals [22] : $C_{11} > 0$; $C_{44} > 0$; $C_{11} - C_{12} > 0$; $C_{11} + 2C_{12} > 0$

3.14. Differents mechanical parameters

Using the elastic constants, other parameters related to elastic properties are determined.

Table 4 shows the elastic anisotropy factor A, the modulus of elasticity B, the Cauchy pressure CP, Young's modulus E, Reuss' shear modulus (Gr), Voigt shear modulus (GV), shear modulus (G), Poisson's ratio (σ), Kleinman parameter (ζ), Pugh ratio (B/G), the wave modulus PW, shear constant Cs, Lamé constants (λ and μ), compressibility (β), and melting temperature Tm of $ASiI_3$-type perovskites (A=Li, Na, K, Rb, and Cs) that we calculated. The stability of a material is described by the compressibility modulus (B). If B satisfies the condition $C_{12} < B < C_{11}$, then the material is stable [21,22]. The compressibility modulus (B) values obtained for NaSrBr3 and $NaSrI_3$ satisfy this latter condition. They are therefore stable. A material is isotropic if its anisotropy factor A is equal to 1. It is anisotropic if the anisotropy factor A is different from 1. In our work, the values of A obtained for $NaSrBr_3$ and $NaSrI_3$ are well above 1. These are therefore anisotropic materials. Young's modulus (Y) describes the stiffness of a material. The material is rigid if it has a high value, but weak if the material is not very rigid. The Y values obtained indicate that $NaSrI_3$ is more rigid than $NaSrBr_3$. To qualitatively estimate the brittle or ductile behavior of a material, we must use the Pugh ratio, i.e., $\frac{B}{G}$ [23]. A Pugh ratio value of 1.75 separates the ductile and brittle characteristics of the material [23]. The material will be brittle if $\frac{B}{G}$ is less than 1.75. It will be ductile if $\frac{B}{G}$ is greater than 1.75. In this study, $NaSrBr_3$ has a $\frac{B}{G}$ value of 19.28, which is well above 1.75. $NaSrI_3$ also has a $\frac{B}{G}$ ratio greater than 1.75, namely 2.69. We can therefore conclude that both materials are ductile, but $NaSrBr_3$ is more ductile than $NaSrI_3$. When studying the characteristics of bond forces, Poisson's ratio σ is used [24]. It is always below the limit value of 0.50. When σ is 0.25, the material in question is ionic [24]. When σ<0.1, the material is covalent. Ductile materials are characterized by a high Poisson's ratio, i.e., σ greater than 0.26. The σ value obtained in this work for $NaSrBr_3$ is 0.47 and that for $NaSrI_3$ is 0.33. This confirms a certain ductility for these materials. The Kleinman parameter ζ is used to quantify internal stress [25]. It characterizes the relative ease of bending the bond versus stretching the bond. When ζ=0, bending of the bond is minimized. When ζ=1, stretching of the bond is minimized. We obtained a ζ value of 0.99 for the perovskites $NaSrBr_3$ and $NaSrI_3$. These values are very close to 1. These materials therefore show greater resistance to bond bending and bond angle distortion. They are also likely to exhibit lower resistance to pure shear deformation compared to unidirectional compression.

Table 2 Calculated other mechanical parameters for cubic $NaSrX_3$ perovskites

Parameters	**Symbol**	**$NaSrBr_3$**	**$NaSrI_3$**
Elastic constants	C_{11} (GPa)	104.60 38.45 [10]	52.14 30.91 [11]
	C_{12} (GPa)	103.32 3.50 [10]	51.45 4.10 [11]
	C_{44} (GPa)	15.01 2.65 [10]	63.84 2.04 [11]
Mechanical stability criteria	$C_{11}+2\ C_{12}$ (GPa)	311.25 -	155.04 -
	C_{11}-C_{12} (GPa)	1.28 -	0.69 -
	$\frac{C_{11}}{C_{12}}$	1.01 -	1.01 -
	$\frac{C_{11}}{C_{44}}$	6.96 -	0.81 -
Anisotropy factor	A	1.27 0.15 [10]	3.44 0.15 [11]
Voigt bulk moduli	B_v	20.20 15.15[10]	41.76 13.35[11]
Voigt shear moduli	Gv (GPa)	9.26 8.08 [10]	38.45 -
Reuss shear moduli	Gr (GPa)	1.50 2.82 [10]	0.86 -
Shear modulus	G (GPa)	5.38 7.92 [10]	19.65 4.84[11]
Bulk modulus	B (GPa)	103.75 15.15[10]	51.68 13.03[11]
Cauchy pressure	C_P (GPa)	88.32 0.85[10]	-12.40 2.06 [11]
Young's modulus	Y (GPa)	0.62 16.59 [10]	1.79 -
Shear constant	C_S (GPa)	0.64 17.48 [10]	0.35 13.41 [11]
Poisson's ratio	σ	0.47 0.32 [10]	0.33 0. 30 [11]
Kleinman parameter	ζ(GPa)	0.99 0.24 [10]	0.99 0.29 [11]
Pugh's ratio	$\frac{B}{G}$	19.28 2.41 [10]	2.63 2.69[11]
Hardness	H_v	0.01 -	0.08 -
Compressibility	β	0.01 -	0.02 -
Isostatic modulus of elasticity	K	1.70 -	1.77 -
Isothermal compressibility	X_T (GPa^{-1})	0.59 -	0.57 -
P-Wave modulus	P_W(GPa)	12.40 23.54[10]	40.62 17.03 [11]
Lamé constant	λ (GPa)	1.64 10.95[10]	0.09 7.35 [11]
Lamé constant	μ (GPa)	1.32 6.30[10]	0.67 4.91 [11]
Melting Temperature	T_m ± 300 (K)	1172.29 781.27[10]	862.21 736.71[11]

Hardness provides insight into the elastic and plastic properties of a compound. The hardness obtained is 0.01 GPa and 0.80 GPa for $NaSrBr_3$ and $NaSrI_3$, respectively. This is a rather low hardness for each material. The ability of a material to resist compression and elongation in the direction of mechanical wave propagation is measured by the PW wave modulus. A high PW value indicates a rigid material. In this case, additional force will be required to deform the material [26, 27]. We obtained PW values of 12.40 GPa and 40.62 GPa for $NaSrBr_3$ and $NaSrI_3$, respectively. The solid phase and liquid phase coexist in equilibrium at a given pressure at the melting temperature. The melting temperature of a material indicates the applicable upper temperature limit [28]. In our study, it is 1172.29 K ie. 999.14 °C for $NaSrBr_3$ and 736.71 K ie. 563,56 °C for $NaSrI_3$. $NaSrBr_3$ will withstand high temperatures better than $NaSrI_3$.

4. Conclusion

This study enabled the determination of the structural, electronic, optical, and elastic properties of $NaSrX_3$ perovskite materials (X=Br and I) using the DFT method with the GGA approximation. The lattice parameters obtained for $NaSrBr_3$ and $NaSrI_3$ are 5.22 Å and 5.74 Å, respectively. The gaps obtained from the electronic band structures are 2.51 eV and 1.49 eV for $NaSrBr_3$ and $NaSrI_3$, respectively. Both exhibit semiconductor behavior. However, with band overlap in the band gap, $NaSrI_3$ is almost a conductor. Both have direct gaps on the Γ-Γ path of the Brillouin zone. These materials are potential optoelectronic and electronic devices. Regarding optical properties, observation of the different optical functions shows that the materials can slow down an incident electromagnetic wave and deflect it in both the visible and ultraviolet ranges. Light can also be absorbed in energy ranges corresponding to the visible and UV. In addition, they will be transparent between 10 eV and 20 eV. These two materials have almost the same reflectivity values. This study also sheds light on the elastic parameters of $NaSrBr_3$ and $NaSrI_3$. The elastic constants found verify the mechanical stability criteria. NaSrBr3 and NaSrI3 are ductile according to Pugh's report. They are likely to be ionic. They are therefore anisotropic and stable materials. These materials show greater resistance to bond bending and bond angle distortion. $NaSrBr_3$ has a higher melting point than $NaSrI_3$. $NaSrBr_3$ will be more resistant to high temperatures than $NaSrI_3$. This work confirms that $NaSrBr_3$ and $NaSrI_3$ materials have very good electronic, optoelectronic, elastic, and optical properties. Their use in a photovoltaic cell could increase its conversion efficiency and also provide excellent stability.

Compliance with ethical standards

Acknowledgments

We would like to thank the Physics Department at Jean Lorougnon Guédé University (UJLoG) in Daloa and the Fundamental and Applied Physics Laboratory (LPFA) at Nangui Abrogoua University (Abidjan, Ivory Coast) for their collaboration in this study.

Disclosure of conflict of interest

No conflict of interest to be disclosed.

References

[1] Geisz J F, Ryan M F, Schulte K L, Myles A S. Six-junction III–V solar cells with 47.1% conversion efficiency under 143 Suns concentration. Nature Energy, vol. 5, no 4, avril 2020, p. 326–335 (ISSN 2058-7546, DOI 10.1038/s41560-020-0598-5).

[2] Renee Gastineau. Engineering a better solar cell: UW research pinpoints defects in popular perovskites [Internet]. Washington: University of Washington; © 2015 [cited 2025 Oct 03]. Available from: https://www.washington.edu /news/2015/04/30

[3] Grancini G, Roldán-Carmona C, Zimmermann I, Mosconi E, Lee X, Martineau D, Narbey S, Oswald F, De Angelis F, Graetzel M, Nazeeruddin M K. One-Year stable perovskite solar cells by 2D/3D interface engineering. Nature Communications8, 15684 (2017). https://doi.org/10.1038/ncomms15684.

[4] Giannozzi P, Andreussi O, Brumme T, Bunau O, Buongiorno N M, Calandra M, Car R, Cavazzoni C, Ceresoli D, Cococcioni M, Colonna N, Carnimeo I, Dal Corso A, de Gironcoli S, Delugas P, DiStasio Jr R A, Ferretti A, Floris A, Fratesi G, Fugallo G, Gebauer R, Gerstmann U, Giustino F, Gorni T, Jia J, Kawamura M, Ko H-Y, Kokalj A, Küçükbenli E, Lazzeri M, Marsili M, Marzari N, Mauri F, Nguyen N L, Nguyen H-V, Otero-de-la-Roza A, Paulatto L, Poncé S, Rocca D, Sabatini R, Santra B, Schlipf M, Seitsonen A P, Smogunov A, Timrov I, Thonhauser T, Umari P, Vast N, Wu X, Baroni S. Advancd capabilities for materials modelling with Quantum ESPRESSO. Phys.: Condens. Matter, 2017, 29, 465901.

[5] P Giannozzi, S Baroni, N Bonini, M Calandra, R Car, C Cavazzoni, D Ceresoli, G L Chiarotti, M Cococcioni, I Dabo, A Dal Corso, S Fabris, G Fratesi, S de Gironcoli, R Gebauer, U Gerstmann, C Gougoussis, A Kokalj, M Lazzeri, L Martin-Samos, N Marzari, F Mauri, R Mazzarello, S Paolini, A Pasquarello, L Paulatto, C Sbraccia, S Scandolo, G Sclauzero, A P Seitsonen, A Smogunov, P Umari, and R M Wentzcovitch. Quantum espresso: a modular and open-source software project for quantum simulations of materials. Journal of Physics: Condensed Matter. (2009), 21(39), p. 395502.

[6] A M Rappe, K M Rabe, E Kaxiras and J D Joannopoulos. Optimized pseudopotentials. Phys. Rev. B 44, (1991), 13175.

[7] J P Perdew, K Burke, K and M G Ernzerhof. Generalized Gradient Approximation Made Simple. Phys Rev Lett. 77(1996)3865 and Phys Rev Lett. 78(1997)1396.

[8] [A D Becke. Density-functional exchange-energy approximation with correct asymptotic behavior. In: Physical Review A, (1988), 38(6), p. 3098–3100.

[9] J P Perdew, K Burke and M Ernzerhof. Generalized Gradient Approximation Made Simple. [Phys. Rev. Lett. 77, 3865 (1996)]. In: Physical Review Letters, (1997), 78(7), p. 1396-1396.

[10] Hossain M T, F-T Zahr, R A-A Dhroobo, Md M Hasan, Md R Al Amin, F M A Sieam, S Swargo, S T Disha, R Islam. First-principles insights into the structural, mechanical, electronic, optical, and thermophysical properties of XSrBr3(X = Na, Ga, and Tl) perovskites: Implications for optoelectronic applications. Materials Science in Semiconductor Processing 182 (2024) 10869.

[11] Hossain M T, Tasmi A, Jahirul I, Md Al-A B Shuvo a, K Hossain, Md A Hossain. Investigation of structural, mechanical, electronic, optical, and thermodynamic properties of AXI3(A = Li, Na; X = Ca, Sr, and Ba) halide perovskites for emerging energy technologies: A DFT study ; Materials Science in Semiconductor Processing. Volume 188. 2025. 109235.

[12] T Tinyang, S TTonga, I Isah, L P Kenda. Electronic and Structural Properties of an Undoped Sodium Iodide. International Journal of Engineering and Applied Physics (IJEAP) Vol. 4, No. 2, May2024, pp. 971-976. ISSN: 2737-8071

[13] H J Monkhorst and J D Pack. Special Points for Brillouin-Zone Integrations. Physical Review B. (1976). Vol 13. pp 5188-5192.

[14] A Jehan, M Husain, N Sfinac, S N Khana, N Rahman, V Tirthe, R Khand, M Sohaild, A A Rachedg, A Khana. First-principles calculations to investigate structural, elastic, electronic, and optical properties of $XSrCl_3$(X =Li, Na). Optik-International Journal for Lightand Electron Optics 287(2023)171088.

[15] D Dwiriani, M Z Efendi, R Aritonang, T U Lestari. Band gap energy characteristics in materials. Journal of frontier research in science and engineering. 3(2)(2025).

[16] A H Reshak, Z A Alahmed, S Azam. Electronic structure, electronic charge density and optical properties analyses of Rb2Al2B2O7 compound: DFT calculation. Int. J. Electrochem. Sci. 9 (2014) 975–989, https://doi.org/10.1016/S1452-3981(23)07771-4.

[17] J Islam, K Hossain. First-principles simulations to investigate effect of hydrostatic pressure on structural, mechanical, electronic, and optical properties of the AgCdCl3 perovskite. Emergent Mater 6 (2023) 1763–1777. https://doi.org/ 10.1007/s42247-023-00565-1.

[18] A Darvishzadeh, N Alharbi, A Mosavi, N E Gorji. Modeling the strain impact on refractive index and optical transmission rate. Phys B Condens. Matter 543 (2018) 14–17. https://doi.org/10.1016/j.physb.2018.05.001.

[19] J Lelièvre. New lead-free materials based on bismuth: towards lead-like compounds (A,A')(B)O3 et (A,A')(BB')O3. University doctoral thesis. Specialty: Ceramic materials and surface treatments. University of Limoges, France. 2017. 210 p.

[20] M H Benkabou, M Harmela, A Haddoua, A Yakoubia, N Bakia, R Ahmedb, Y Al-Douric, S V Syrotyuke, H Khachaia, R Khenataf, C H Voong, M.R Johanc. Structural, electronic, optical and thermodynamic investigations of NaXF3(X=Ca and Sr): First-principles calculations. Chinese Journal of Physics. 56(2018)131-144.

[21] M Houari, B Bouadjemi, M Matougui, S Haid, T Lantri, Z Aziz, S Bentata and B Bouhafs. Optoelectronic properties of germanium iodide perovskites AGeI3 (A= K, Rb and Cs): 1st principles investigations. In : Springer Nature. (2019). Vol. 51. No. 7. p 1–14.

[22] [M Houari, B Bouadjemi, S Haid, M Matougui, T Lantri and Z Aziz. Semiconductor behavior of halide perovskites AGeX3 (A = K, Rb, Cs; X = F, Cl Br): first-principles calculations. Indian J Phys. (2019). Vol. 97. pp 1-13.

[23] S F Pugh. Relations between the elastic moduli and the plastic properties of polycrystalline pure metals. The London Edinburgh and Dublin Philosophical Magazine and Journal of Science. (1954). Vol 45. No 367. pp 823–843.

[24] A Meziani. Study of the structural, electronic, elastic, and optical properties of CsCdF3 and KZnF3 fluoro-perovskite compounds. University doctoral thesis, Specialization: Condensed Matter Physics. Mokhtar Badj University, Algeria. 2012. 95 p.

[25] B Kleinman, M Karplus; Phys Rev. B 3 (1971) 24.

[26] S Chibani, O Arbouche, M Zemouli, Y Benallou, K Amara, N Chami, M Ameri, M E Keurti. First-principles investigation of structural, mechanical, electronic, and thermoelectric properties of Half-Heusler compounds RuVX (X=As, P, and Sb). Comput Condens Matter 16. (2018) e00312. https://doi.org/10.1016/j.

[27] Mavko G, Mukerji T, and Dvorkin J. (1998) The Rock Physics Handbook: Tools for Seismic Analysis in Porous Media. Cambridge University Press, 208-210.

[28] Q Fan, C Chai, Q Wei, H Yan, Y Zhao, Y Yang, X Yu, Y Liu, M Xing, J Zhang, R Yao. Novel silicon allotropes: stability, mechanical, and electronic properties. J Appl Phys. 118 (2015) 185704, https://doi.org/10.1063/1.4935549.